JOURNAL OF COMPUTATIONAL PHYSICS 11, 507–530 (1973)

A Numerical Method for Studying Liquid Drop Behavior: Simple Oscillation*

G. BRANT FOOTE†

Institute of Atmospheric Physics, University of Arizona, Tucson, Arisona 85721

Received April 24, 1972

A new technique for simulating liquid drop behavior on the computer is described. Sample computations and results are presented for the case of a simple drop oscillation. The computing method is based on an extension of the Marker-and-Cell method, and includes the effects of surface tension in a way similar in several important respects to that of B. J. Daly. The geometry is presently constrained to be axisymmetric. Available theory pertinent to the drop oscillation problem (and sufficient to give a reasonably definitive check on the model's accuracy) is reviewed. For small-amplitude oscillations (to which the theory applies) the agreement between theory and numerical prediction is very good. The predicted characteristics of the large-amplitude oscillation are discussed.

INTRODUCTION

There are a variety of phenomena, both in nature and in industry, which involve the interactions of an assemblage of liquid drops with one another, with other surfaces, and perhaps with an atmosphere. Obvious natural examples are the growth of raindrops by the coalescence of colliding drop pairs, the unstable breakup of large falling drops caused by their interaction with an air stream, and the splashing and erosion produced by raindrops impacting on soil. Similar examples can be found in various industrial processes.

While there are some situations in which one can treat liquid drops as being rigid spheres (e.g., the raindrop collision efficiency problem), one sees from the examples above that there are important cases for which the deformation of the drop produces the effect under consideration. It is clear from the difficulties inherent in dealing with nonlinear fluid flows involving free surfaces, particularly when surface tension is present, that a numerical approach offers the best oppor-

* This research was sponsored in part by the Atmospheric Sciences Section of the National Science Foundation under Grant GA-24134.

† Present affiliation: National Center for Atmospheric Research, Boulder, CO 80302.

tunities for the theoretical study of general drop distortions. In this paper we present a numerical technique which has been successfully used for simulating liquid drop behavior. To establish the model's accuracy and applicability we present the results of calculations simulating the lowest-order oscillations of a drop, and compare those results with available theory.

Basic Computing Scheme

The basic scheme used here for integrating the equations of fluid motion is that of the Marker-and-Cell (MAC) method, developed by the Los Alamos group [11]. It utilizes the full Navier–Stokes equations for an incompressible, viscous fluid, and is particularly suitable for problems involving free surfaces. Very briefly, the MAC method integrates the finite-difference form of the Navier–Stokes equations subject to appropriate boundary conditions. Velocity components and pressure are defined over a staggered Eulerian mesh. A Lagrangian system of marker particles is defined, and these markers are moved through the grid at interpolated local fluid speeds, behaving much like dye particles in acual experiments. As time progresses, the positions of these marker particles serve to specify the location of the fluid surface, and hence, can define in which computing "cells" the surface boundary conditions should be applied. The MAC method is well documented elsewhere [6, 11, 12, 28], and the reader is referrred to other publications for further details. Except as specifically noted, the techniques used here are those of the original MAC method.

The drop calculations made here have been restricted to two-dimensional axisymmetric geometry, appropriate to the drop problem. Despite the apparent limitations of two dimensions, a variety of realistic drop phenomena can be so studied. In addition to the simple oscillations reported here, the dynamics of a drop impacting on a wall (equivalent to the collision of equal-size drops along their line of centers), and the disruption of a highly electrically stressed drop have been successfully simulated. This other work is being reported elsewhere.

Surface-Tension Effects

In order to simulate liquid drop behavior one must, of course, account for the effects of surface tension. If we let r_1 and r_2 denote the principal radii of curvature of the surface of a drop at a given point, then the pressure difference across the interface there is given by Laplace's formula

$$p - p_0 = \sigma(1/r_1 + 1/r_2), \tag{1}$$

where p is the pressure just inside the surface, p_0 is the pressure just outside the drop (atmospheric pressure, for example), σ is the surface tension coefficient, and both r_1 and r_2 are reckoned positive when drawn into the drop {for derivation see, e.g., Landau and Lifshitz [16]}. As long as we are not concerned with contact-angle considerations, then incorporation of the surface pressure condition (1) is the only modification necessary for the inclusion of surface-tension effects in fluid flow problems. The actual method used here for including this conditions will be discussed later. For general surfaces the determination of the two radii of curvature would be extremely difficult, but in the present work we deal only with surfaces of revolution, and for this case the two radii can be specified relatively simply.

Let the drop profile shown in Fig. 1 be given by the relation $z = z(r)$. We will

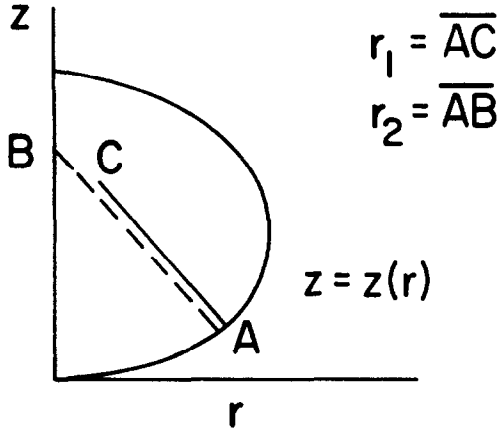

FIG. 1. Drop profile showing the two principal radii of curvature.

consider presently the complications arising from the double-valued nature of this function. The curvature in the plane of the figure is given by the usual equation

$$1/r_1 = z''/(1 + z'^2)^{3/2}, \tag{2}$$

where r_1 is the distance $\overline{AC}$ in Fig. 1. The second curvature required is that of the trace of the drop surface in that plane perpendicular to both the plane of the figure and the tangent plane at the point in question. Since we deal with a figure of revolution, it is clear that the distance AB in Fig. 1, where point B lies on the z axis, is the required radius r_2. One can easily show that

$$1/r_2 = z'/r(1 + z'^2)^{1/2}. \tag{3}$$

This curvature is the same as that of a cone tangent to the drop at A, and with apex on the z axis.

A complication now arises from the specific geometry of the drop problem: In spite of the fact that the surface curvature remains finite everywhere, at the drop's equator the slope, dz/dr, of the profile becomes infinite, and Eqs. (2) and (3) cannot be used for numerical computation. In the present work the resolution of this difficulty has been simply to switch the role of ordinate and abscissa in the vicinity of the drop equator, so that the new slope there, dr/dz, is of order unity. While this increases the computer programming complexity, it creates no formal difficulty. Daly [5] has utilized the same artifice in his work. An attractive alternative to this procedure of interchanging ordinate and abscissa is to define the drop profile in parametric form, $r = r(s)$, $z = z(s)$, for then the above-mentioned difficulties do not arise. Drop-related calculations employing such a parametric formulation have been reported in the literature [2, 26]. The present method is completely workable, however, and the principal gain from using a parametric representation comes from the programming simplifications.

Evaluating Surface Curvatures

We now consider the problem of specifying the surface location with sufficient accuracy to evaluate the derivatives involved in calculating the two radii of curvature from Eqs. (2) and (3). The general approach used in the present study is patterned after the work of Daly [5], who applied the technique to a study of the two-fluid Rayleigh–Taylor instability.

In the original MAC calculations, the surface is specified as being a region of surface cells, and, as such, is only resolved by the fixed Eulerian mesh. Such resolution is, of course, too crude to allow evaluation of curvatures. Daly [5] has introduced the idea of using the MAC Lagrangian coordinate system of marker particles to describe the surface location with more accuracy. At some initial time an ordered sequence of marker particles is laid out along the nominal surface. As the flow develops, these surface particles, as we will call them, are moved at the local fluid speed, and thereafter mark the position of the surface. The spacing of these particles is of some importance, and the present experience in this regard will be discussed later. Daly's procedure then involves determining the actual surface curvature from the orientation of an interpolation curve passed through the surface particle array. In particular, a cubic spline is employed. This procedure not only ensures that the surface curvature will vary smoothly from point to point (an important stability consideration), but provides a means for evaluating the necessary derivatives anywhere on the nominal surface.

It should be pointed out that for simple flows (such as the one to be discussed here), surface tension is most easily incorporated into a model using purely Lagrangian finite difference techniques {see, e.g., Hirt, Cook and Butler [13]}.

For flows undergoing large distortion, however, purely Lagrangian techniques have a rather limited applicability. The present interest in developing a method which can be applied to a study of drop breakup and coalescence has led to the more complicated framework presented here.

The Spline Curve

The cubic spline fitted to a given array of points consists of sections of cubic polynomials joining each adjacent pair of points such that slopes and curvatures are continuous at the junctions. In the present case, the given points are taken as the locations of the surface particles. Consider an ordered sequence of n points (x_i, y_i) which is monotonic in x. One seeks to determine the spline approximation curve, $y(x)$, which has second derivative M_k at point $x = x_k$. We specify that y'' vary linearly between points x_{k-1} and x_k:

$$y''(x) = M_{k-1}[(x_k - x)/h_k] + M_k[x - x_{k-1})/h_k], \tag{4}$$

where $h_k = x_k - x_{k-1}$. Upon integrating this equation once and requiring that the first derivatives be continuous at the junction points one obtains a set of equations for the M's:

$$\begin{aligned}(h_k/6)\, M_{k-1} + [(h_{k+1} + h_k)/3]\, M_k + [(h_{k+1})/6]\, M_{k+1} \\ = [(y_{k+1} - y_k)/h_{k+1}] - [(y_k - y_{k-1})/h_k]\end{aligned} \tag{5}$$

(see Ref. [27]). This set of $n - 1$ equations, along with two end conditions is sufficient to determine the unknown quantities M_k. A stable explicit algorithm for inverting the resulting tridiagonal matrix has been given by Peaceman and Rachford [22].

Spline Boundary Conditions

The boundary conditions used by Daly [5] were simply that $M_0 = M_1$ and $M_n = M_{n-1}$. In addition, the first and last points were placed so that the spline curve intercepted the boundary at the desired angle. The same procedure is appropriate here at the upper and lower poles of the drop. Thus, the first particle (x_1, y_1) is placed just inside the computing region, a small distance away from the z axis. The zeroth particle is then placed at $x_0 = -x_1$, and $y_0 = y_1$, in proper axisymmetry with the first. [Note that we are here making the correspondence of (x, y) with (r, z). When we later deal with a subsequence of particles near the drop equator we interchange ordinate and abscissa and instead make the correspondence (x, y) and (z, r).]

In the drop problem, unless a parametric formulation is used, it is always necessary to break the surface array up into three monotonic subsequence of surface particles, and compute separately the spline curves for each. Starting from the lower pole of the drop, the first subsequence is monotonic increasing in r, the second increasing in z, and the third decreasing in r. For each of these subsequences at least one end point of the spline does not lie on the z axis, and in this case a different boundary condition has been used here. Let (x_j , y_j) be the end of the first subsequence. This break-point is determined by examining the slopes of straight line segments joining adjacent surface particles and finding where this slope becomes greater than one. The tangent of the drop profile at (x_j , y_j) is thus very close to unity. Now at such a break-point the condition $M_{j+1} = M_j$ is not a good one. For a sphere, for instance, this is just the region where the slope, and hence M also, is starting to attain large values, whence the array experiences large particle-to-particle changes in M. In this case it is the curvature which should actually remain constant. Daly's method involves making the spline go through the next point (x_{j+1} , y_{j+1}) with $M_{j+1} = M_j$. We do two different things. First, we constrain the spline curve to go through the next *two* points after the break-point, so that the boundary condition is applied to M_{j+2} but we only use M values up to M_j . This transfers the roughness away from the region where curvatures are actually evaluated. The calculations of adjacent splines thus overlap, and five particles are common to both spline fits, two on either side of the break-point. Second, we use a more accurate boundary condition at the end point. We sense that it is desirable to keep the curvature constant rather than M constant, and approximate this condition by maintaining the first radius of curvature r_1 constant. Thus, at an interior spline end point (x_p , y_p), where $p = j + 2$, we have the boundary condition

$$[y''/(1 + y'^2)^{3/2}]_p = [y''/(1 + y'^2)^{3/2}]_{p-1} . \tag{6}$$

Now for y_p'' we naturally use M_p . But for the slopes we make the approximation

$$y_p' = (y_{p+1} - y_{p-1})/(x_{p+1} - x_{p-1}), \tag{7}$$

so that we arrive at the boundary condition

$$M_p = M_{p-1}[(1 + y_p'^2)/(1 + y_{p-1}'^2)]^{3/2}, \tag{8}$$

where the slopes are evaluated from the centered difference formula (7). Use of the condition (8) has given very satisfactory results, and has greatly reduced the presence of spurious curvatures in the civinity of spline sub-sequence end points.

Equations (2) and (3) are appropriate for computing curvatures when dealing with a sub-sequence monotonically increasing in r, such as in the present case, the lower surface of the drop. Over the upper surface, where the sequence is

decreasing in r, the convention that the curvature be positive when the radii are drawn into the drop requires that the negative of the values given by (2) and (3) be used.

For a subsequence monotonically increasing in z we use z as the abscissa ($x = z$) and r as the ordinate ($y = r$). The proper relations are then

$$1/r_1 = -r''/(1 + r'^2)^{3/2}, \tag{9}$$

$$1/r_2 = 1/r(1 + r'^2)^{1/2}. \tag{10}$$

Evaluation of Surface Pressure

In Daly's two-fluid calculations, it was convenient to include surface-tension effects as a force term in the equations of motion. In the present work, unlike Daly's, explicit boundary conditions on pressure are applied at the drop surface during the relaxation solution of an elliptic equation for the pressure field. Thus, the natural procedure for including the surface-tension stress is to evaluate the pressure for each surface cell from Eq. (1) each time step, and then keep these surface boundary values fixed during the relaxation process. Prior to this, of course, one must at each time step make new spline fits to the newly positioned array of surface markers, arriving at updated M values necessary for evaluating curvatures and the spline position.

Since, in general, the spline curve will not go through the center of a given cell, where the pressure is defined, it is necessary to mention where the surface curvature is actually evaluated. The procedure used in the calculations reported here is relatively simple. The radii of curvature used in (1) are *evaluated* at the points where the spline enters and exits a given cell. The resulting pressures computed for these two points are then averaged and *applied* at the cell center. While this scheme appears to be rather arbitrary, it seems to give better results than other similarly simple methods that have been tried here. In particular, since adjacent surface cells share a common pressure evaluation at their common boundary, use of this evaluation scheme tends to keep the surface pressure distribution smooth, an important stability consideration.

It will occasionally happen that a surface cell will just miss being penetrated by the spline curve. In this case an alternate routine assigns the cell a surface pressure by using the curvature of the spline at its point of closest approach to the cell center in question. In stable calculations, such an event will occur only rarely.

Further details on the actual logic required for the surface pressure evaluation (including the complication that one must subdivide the array of surface particles and deal with each subsequence separately) are given by Foote [8].

Modifications of the Surface–Pressure Treatment

It is recognized that the method of applying the surface–pressure boundary condition at the center of the surface cell, rather than at the surface itself, will lead to error. Other investigators making MAC calculations have attributed a slight waviness on the free surface, with a scale on the order of the mesh interval, to the fictitious accelerations which result from this procedure [3, 13, 21]. In some cases it has been noted that this surface noise will amplify and eventually mask the real motion [3]. In the present work, however, it is found that the more or less random character of this error, which, of course, depends on the relative size of the mesh interval used, does not appear to affect the gross fluid motion.

Methods have been proposed by Chan and Street [3] and by Nichols and Hirt [21] for applying the normal stress condition more accurately, and in particular, at the location of the surface rather than the center of the surface cell. Chan and Street's technique of "irregular stars" involves the use of irregular leg lengths in the definition of a finite-difference Laplacian operator. The use of these irregular stars for appropriate surface cells during the iterative solution of an elliptic, equation for pressure seems to offer definite advantages over other methods, particularly with regard to accuracy and stability, but its incorporation into existing MAC computing codes is not straightforward. In addition, the method makes rather extravagant use of computer storage. For example, the only alternative to storing four additional fields (four leg lengths for each cell) would be the time consuming development of rather complicated programming logic.

The method of Nichols and Hirt [21] is more easily adapted to existing MAC programs. It involves making a linear estimation of the surface-cell pressure from a knowledge of the pressure at the actual surface and the pressure of an adjacent full cell.

If p_a is the pressure at the actual surface (sum of the applied external pressure and the contribution from the normal stress condition), then the estimated pressure p_s at the center of the surface cell is given by Nichols and Hirt as

$$p_s = p_1 + ((p_a - p_1)/D)h, \tag{11}$$

where h is the mesh size, p_1 is the pressure of the adjacent full cell, and the other symbols are defined in Fig. 2. (In this figure the interpolation is assumed to be in the r direction. The usual procedure is to extrapolate from a direction as normal to the surface as possible. Thus, in the upper and lower regions of the drop one extrapolates in the z direction. Near the drop equator one extrapolates in the r direction.) As noted by Nichols and Hirt, difficulties arise with the use of (11) when the distance D becomes too large or too small. A variant of this method which has been tested here gets around this problem:

$$p_s = p_a + [(p_1 - p_2)/h]d. \tag{12}$$

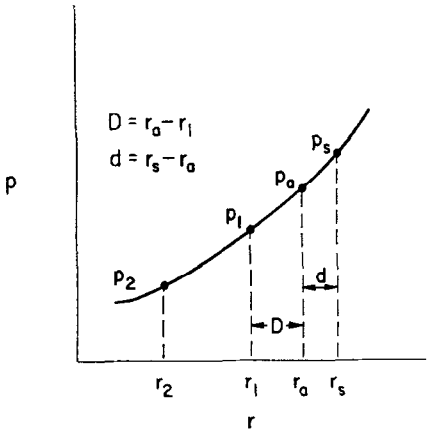

FIG. 2. Definition sketch for quantities appearing in Eqs. (11) and (12). The distances r_1, r_2, and r_s correspond to cell centers; r_a indicates the position of the actual surface.

The stability of a relaxation procedure when used in conjunction with (12) is not sensitive to the magnitude of d. Another difficulty with (11) that doesn't arise with (12) occurs when a given surface cell does not have a neighboring full cell from which to extrapolate, a situation which can happen occasionally. In this case the pressure p_1 will itself be extrapolated, and while (12) still converges, it is observed here that (11) generaly fails to do so. The fact that (12) is of lower-order accuracy than (11) is overridden by its better stability characteristics.

Test problems conducted here using (12) have noted some improvement over parallel calculations with the original MAC method regarding the smoothness of the free surface. However, the improvement has not always been substantial, and the calculations discussed later in this paper have been made with the original method. As will be seen, the results appear to be quite satisfactory.

SURFACE PARTICLE SPACING

The spacing of the surface particles proves to be an important consideration in making a successful computation. If the particles are too far apart the surface is not well resolved, and the results may not be very accurate. If the spacing is too close, small fluctuations in particle position will generate faulty curvatures, eventually causing amplifying errors. In the present work it has been found necessary to keep the particle separation in the range 1–2.25 h, where h is the mesh interval. It is interesting to note that Daly's [5] spacing of 0.4 h has not been workable in the drop study, and has led to ficticious surface "noise." The particles are initially laid out with a separation of 1.25 h to about 1.5 h, but as a result of

the surface stretching and shrinking accompanying the drop motion, this separation may later change. Following Daly, a procedure is adopted which adds or deletes particles from the surface array each time step as necessary to keep the spacing with the proper bounds. If the spacing were initially the same as the grid interval, which of course would be desirable, there would be no latitude for surface shrinking, and undesirable spacings less than h could immediately occur.

If two particles are found to be too close together, then a test is made to see which is closest to its other neighbor, and this is the one deleted.

When the spacing between two adjacent particles becomes too great then a new particle is inserted between. Its position is initially taken to be midway between the two. However, this straight profile will almost never fit the general shape of the surface. The particle is smoothed to try to bring it into alignment. The smoothing consists of fitting a least-squares parabola to five points, namely, the points marking the position of the new particle and the positions of the two nearest particles on either side. The ordinate of the new particle is then adjusted to lie on the parabola. This procedure is also taken from the work of Daly [5]. As the present work has progressed, however, close checking has revealed that even after one smoothing the M value of the new particle is spurious—indicating that the new particle still does not fit the general run of the curve. One further smoothing solves the problem, and in the current version of the drop model all added particles are smoothed twice before the computations proceed.

Smoothing the Surface

Daly [5] has found it useful to smooth occasionally certain surface particles that become irregularly placed as the flow develops. As he points out, the chief difficulty involved in treating this problem lies in actually detecting the irregularity. Daly's criterion involves smoothing the kth particle whenever M_k exceeds a predetermined value. Experience in the present work has been that large particle-to particle changes in the M's, rather than simply large M values tend to generate surface noise. A smoothing scheme which was thought to be useful in the early stages of this work is the following. A given surface particle is smoothed whenever its M value differs from the average of its two neighbors by an amount proportional to some typical curvature, in the present case $1/r_e$, where r_e is the radius of the sphere having the same volume as the drop. This technique is extremely sensitive to short-wavelength perturbations of amplitude much smaller than can be detected by eye in particle position plots. The smoothing technique employed is the same as that discussed earlier in the context of adding particles, and involves a least-squares quadratic.

In fact, as a variety of drop motions have been studied with the present program,

it has become apparent that any artificial smoothing of the surface array is detrimental. Even though smoothing in this way frequently reduces the running time on the computer, by reducing the amount of time needed for convergence of the pressure equation, its use eventually causes short-wavelength surface perturbations to develop. While these perturbations do not always amplify, their presence is not desirable and the best results have been obtained with no artificial smoothing.

Numerical Stability

The computational stability of the MAC method has been discussed by various authors [3, 6, 12, 28]. Analysis of linearized equations leads to the usual conditions on the time increment, δt:

$$\delta t < \delta x/c, \tag{13}$$

$$\delta t < \delta x^2/2\nu, \tag{14}$$

where δx is the mesh width, c is the maximum fluid speed, and ν is the kinematic viscosity. The speed of propagation of plane capillary waves is given by

$$u = [2\pi\sigma/\rho\lambda]^{1/2}, \tag{15}$$

where λ is the wavelength, and ρ is the fluid density. According to (15), the highest wave speed corresponds to the smallest resolvable wavelength, i.e., $\lambda = 2\delta x$.In fact, it can be shown that the group velocity U of capillary waves is given by $U = 3u/2$. In the present work it has been found necessary to satisfy (13) with c taken as the $2\delta x$ group velocity, even though actual fluid speeds are generally an order of magnitude smaller. Any violation of this criterion soon leads to amplifying surface waves.

Hirt [12] and Daly and Pracht [6] have discussed a method for analyzing nonlinear instabilities, that is, computational instabilities resulting from the presence of nonlinear terms in the differential equation. The method involves expanding each term in the corresponding difference equation in a Taylor series, and retaining only the terms of the original differential equation and the resulting diffusion-like truncation terms to order δt and δx^2. In so doing, one finds it possible to group together certain factors of these truncation terms with the kinematic viscosity as coefficients of the original diffusion terms (the reader is referred to the original papers for details). These coefficients may then be interpreted as an effective viscosity coefficient, as used by the difference equations. In order that the difference solutions remain stable, this effective viscosity must remain positive, leading to the approximate stability condition

$$\nu > 1/2\ \delta x^2\ \partial u/\partial x, \tag{16}$$

where $\partial u/\partial x$ is the maximum velocity gradient in the direction of flow. This analysis gives interesting insights into why trouble should develop in regions of large velocity gradients, a fact pointed out by Philips [23], who first discussed the nonlinear instability phenomenon. Thus, Hirt's analysis shows how the presence of large velocity gradients can lead to truncation errors which tend to amplify local anomalies in the flow fleld, rather than smooth them out. Condition (14) also shows the difference solutions will be unstable for negative values of ν. From Phillips viewpoint, however, one sees that the high wave-number components in the Fourier representation of a given variable (corresponding to large gradients) can be aliased back to lower wave numbers by the nonlinear terms of the finite-difference equation, eventually causing a nonphysical increase in kinetic energy which can dominate the motion. It is clear that the phenomenon discussed by Hirt does not possess this amplifying character, for it can be shown by the methods of Lilly [17] that the nonlinear terms of the MAC difference equations conserve kinetic energy (except near boundaries). Thus, while the type of staggered grid used in the MAC method does not eliminate aliasing errors, its use essentially controls nonlinear instabilities. The phenomenon discussed by Hirt is not a nonlinear instability in the sense of prior usage of that term, involving unbounded error growth. But Hirt's method is a useful technique for understanding how to avoid a type of nonlinear bounded error that can, nevertheless, completely distort the flow field and the energy spectrum.

In the present work it has been necessary to keep ν large enough to satisfy (16), and δt small enough to satisfy (13). Condition (14) is found to be less stringent than the other two. As pointed out by Daly and Pracht [6], condition (16) essentially gives an upper limit on the Reynolds number Re of the problem. Observations in the current work have been that when Re becomes too large, surface noise develops (see also Refs. [3], [13], [21]), and for sufficiently large Re will amplify and cause termination of the calculations. Since, as previously mentioned, the MAC method effectively eliminates the unbounded growth of nonlinear instabilities, one suspects that this type of error growth is related to the handling of the free surface. Indeed, since surface tension drives the motion in the drop problem, and since the surface tension stress is calculated from the positions of surface particles, themselves located in the very region where cellular velocities are approximated, it is clear that stable and accurate calculation including surface-tension effects depends strongly on the handling of the free-surface boundary conditions. It is found here that the treatment of the original MAC method is workable, but that further improvements in this regard would be desirable.

While the Hirt analysis is useful for understanding how to avoid a certain class of observed instabilities, it evidently is not able to predict the onset of instability in all cases. For example, Chan and Street [3] performed stable calculations (with a modified version of the MAC method) employing zero viscosity, clearly in

violation of (16). Their success was attributed to an improved handling of the free surface. In particular, they used a heuristic technique for extrapolating fluid velocities across the surface, and employed the method of "irregular stars" previously mentioned. In future calculations it is intended to evaluate these suggested modifications.

Drop Oscillation: Available Theory

Before proceding to the present numerical calculations, it is appropriate to review briefly the main theoretical results pertaining to the drop oscillation problem, with a view toward comparing the numerical prediction with theory.

The nature of the vibrations of a liquid drop about a spheroidal shape was first investigated mathematically by Lord Rayleigh [24]. For the purpose of finding oscillation frequencies, Rayleigh determined that it was sufficient to consider only axisymmetric motion (it can be shown that the three-dimensional modes oscillate with the same frequency as the axisymmetric modes), and one may represent the shape of the drop in spherical coordinates (r, θ, ϕ) as

$$r = R + \sum a_n P_n (\cos \theta), \tag{17}$$

where P_n is the nth order Legendre polynomial, θ is the polar angle, R is the radius of the unperturbed sphere, and the coefficients a_n are functions of time. The potential energy, also called surface energy S_e, available to drive the oscillation is given by

$$S_e = \sigma(A - A_s), \tag{18}$$

where σ is the surface tension coefficient, A is the actual surface area, and A_s is the constant area of the equivalent sphere. By assuming potential flow and only small distortions from a spherical shape, Rayleigh was able to express the kinetic and potential energies as functions of the a_n's. Using Lagrange's method, for which the a_n's become the generalized coordinates, he then obtained the result that $a_n = b_n \cos \omega t$, where b_n is some amplitude, and ω is given by

$$\omega^2 = n(n - 1)(n + 2)(\sigma/\rho R^3), \tag{19}$$

where ρ is the fluid density. We notice that $n = 0$, 1 correspond only to rigid body motion, and the fundamental mode corresponds to $n = 2$.

The four lowest normal modes of vibration are illustrated in Fig. 3. The amplitude of oscillation b_n is the same for each mode, and is expressed in terms of the axial ratio γ of the fundamental (the axial ratio, which is useful in describing the oblate–prolate fundamental mode, is defined here as the ratio of horizontal

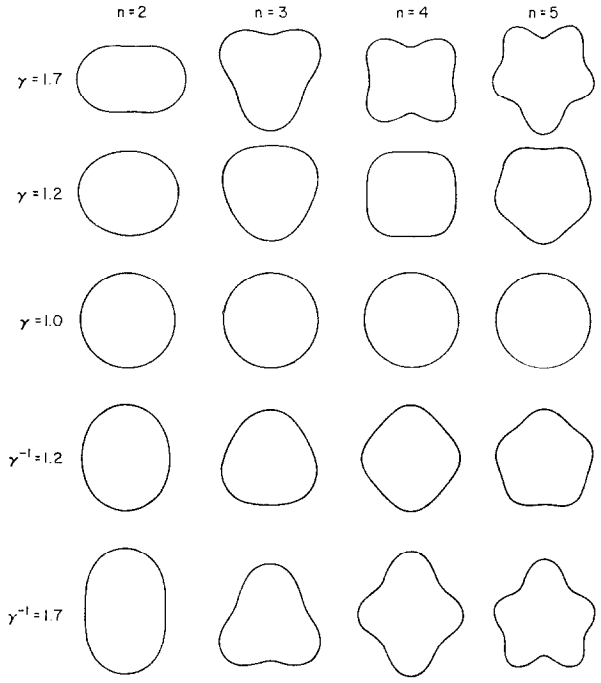

FIG. 3. The four lowest normal modes of an oscillating drop, plotted from Eq. (17).

to vertical axis length). While the Rayleigh theory is strictly valid only for oscillations of small amplitude ($b \ll R$), the fundamental mode shown in Fig. 3 shows a remarkable similarity to actual photographs of oscillating drops. In particular, the profile tends to be somewhat blunt rather than drawn out like an actual ellipsoid.

A more general treatment of the drop oscillation problem has been given by Landau and Lifshitz [16]. By writing an equivalent of (17) in terms of the surface harmonic $P_n^m(\cos\theta)e^{im\phi}$, it is shown that for each n there are $2n + 1$ different oscillations, corresponding to $m = 0, \pm 1, \pm 2, \ldots, \pm n$, all having the same frequency. In fact, for each n there is one axisymmetric mode and only n physically distinct three-dimensional modes, since $+m$ and $-m$ lead to the same oscillation. Thus, for $n = 2$ there are three degenerate modes. The axisymmetric oblate–prolate mode is shown in Fig. 3. The other two modes have in the past been referred to as the transverse-shear mode and the toroidal mode. The transverse-shear mode looks something like a 45° wobble about an axis through the poles, and involves relative opposing motion between the two hemispheres. The toroidal mode gives rise to shapes resembling triaxial ellipsoids, with the major axis oscillating between

two perpendicular directions in the equatorial plane, and with no radial movement at the poles.

The toroidal mode has been frequently observed in wind tunnel studies of suspended large drops, although to this writer's knowledge never properly identified (see Refs. [1, 7, 9, 18, 20]). Apparently large drops (for water, greater than 4 or 5 mm in diameter, for example), which are greatly flattened on the bottom when supported at terminal speed in an air stream, find it easy to oscillate with only longitudinal components that do not require vertical pulsations. (It has, in fact, been observed that sessile drops can also be excited to oscillate in this mode). The "wobbling" mode and the oblate–prolate mode (or "pulsation" mode, as it as been called) are commonly observed for all sizes. Since the air flow around a suspended drop tends to be axisymmetric, the axisymmetric modes are understandably the most frequently observed, and, in any case, are the most easily identified.

The above analysis does not include the effects of viscosity. For small viscosity ($\nu/\omega R^2 \ll 1$) Lamb [14, 15] has shown that the only viscous effect is that of gradually reducing the amplitude of oscillation. In particular, the period is not changed. If b_0 is the initial amplitude, and b is the amplitude after time t, then Lamb's result can be expressed as

$$b = b_0 e^{-\beta t} \tag{20}$$

where β is given by

$$\beta = (n - 1)(2n + 1)\nu/R^2. \tag{21}$$

The ratio b/b_0 is plotted in Fig. 4 for the seven lowest modes of oscillation, $n = 2$ to $n = 8$, for water drops (i.e., $\nu = 0.014$ cm^2 sec^{-1}) of various sizes. The uppermost curve is for $n = 2$, and the lower curves correspond to successively higher modes. The abscissa is in units of the fundamental period of oscillation for a drop of the indicated diameter. Thus, viscosity of magnitude corresponding to that of water will reduce the amplitude of oscillation of a 5 mm diameter drop to 10% of its initial value after about 63 oscillations of mode $n = 2$ (for which the period is 32 msec). In contrast, a 100 μm drop will undergo the same damping in only nine oscillations (each with period of only 0.1 msec). Note that the higher-order modes damp out much faster than does the fundamental.

Chandrasekhar [4] has also studied the oscillations of a viscous spheroid, and has obtained more general results (see also Reid, [25]). However, the conclusions for the problem of present interest are the same as those just considered. For fluid viscosities characteristic of water, Eq. (20) should be quite accurate for drops as small as a few hundred microns in size.

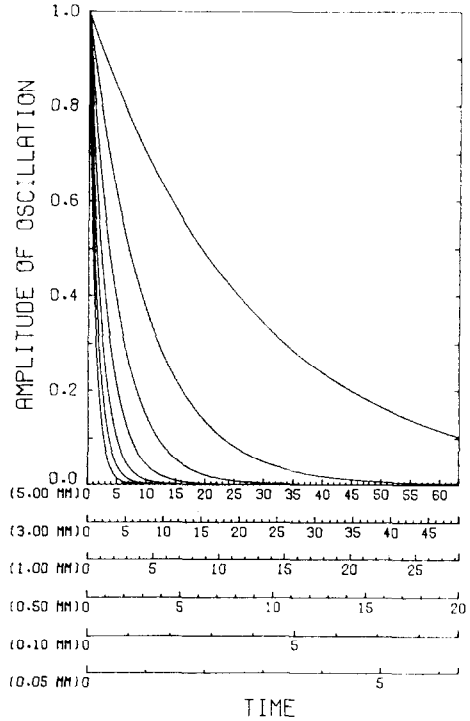

FIG. 4. Fractional reduction in amplitude for the oscillation of a viscous spheroid. The uppermost curve is for an oscillation of mode $n = 2$, and the lower curves correspond to successively higher modes. The abscissa is in units of the fundamental period of oscillation for a water drop of the indicated diameter.

NUMERICAL RESULTS: A SAMPLE COMPUTATION

As an example of the applicability and accuracy of the computing method for simulating drop phenomena, we present here the results of a study concerned with the simplest of all motion of a liquid drop—the oblate–prolate oscillation. Studies of the dynamic impact of two drops and of the electrostatic instability of a charged drop and a drop in an electric field have also been carried out, and will be reported elsewhere. Some of the material may also be found in a dissertation by the author (Ref. [8]). The calculations were made on a CDC-6400 computer and the plotting done on a Calcomp 665 digital incremental plotter.

In order to start the fluid dynamic calculations one requires, along with values of ν and σ, specification of the initial flow field and initial drop shape. The

calculations presented here have been started from rest with two initial shapes: that shape given by the fundamental mode of the Rayleigh theory [the "Rayleigh shape," from Eq. (17)], and that of a true oblate spheroid. Various initial amplitudes have been assumed, with axial ratios γ up to 1.9.

An example of the computed results is shown in Fig. 5, where computer-drawn

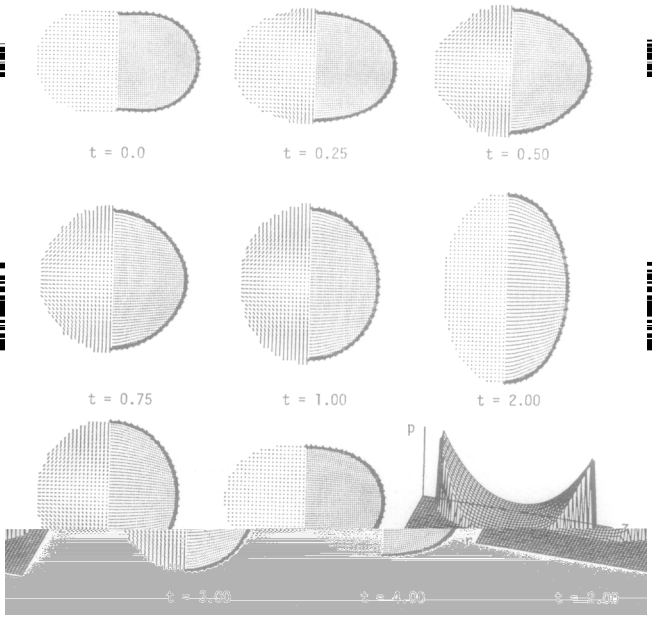

FIG. 5. Computed oscillation of a drop started with the "Rayleigh" shape.

plots are shown for several times. The drop shape is initially that given by the Rayleigh theory, and the pertinent data are as follows: If the drop diameter is taken as $d = 1.2$ mm, then the times given below each plot are in milliseconds, the grid interval is $h = 3.33 \times 10^{-3}$ cm, $\delta t = 8 \times 10^{-6}$ sec, $\nu = 0.06$ cm^2 sec^{-1}, and $\sigma = 75$ dyn cm^{-1}. The oscillation is started with an axial ratio of 1.7, and the full period of oscillation is computed to be 3.97 msec. An enlarged view of the plot for $t = 1.0$ msec is shown in Fig. 6.

Figures 5 and 6 show three types of plots. The right-hand section through the drop shows the configuration of the marker particles, indicated by dots. The positions of surface particles are indicated by small crosses. The left-hand section shows a velocity vector plot. The velocity vector for each occupied cell is drawn simply as a straight line starting from the center of the cell and pointing in the appropriate direction. A zero velocity is plotted as a point. At time $t = 2.0$ msec, Fig. 5 shows the pressure distribution as a function of r and z.

The drop in Fig. 5 is at rest at time zero. As the pressure gradient forces accelerate the fluid, the velocities increase until the drop reaches a spherical shape, near $t = 0.86$ msec (not shown). The velocities then go through a maximum, the drop starts to slow down, and comes momentarily to rest in a prolate configuration near $t = 2.0$ msec. At this time the plotted pressure distribution indicates that the highest pressures occur at the poles, and shows that the drop waist is a region of relatively low pressure, consistent with the surface curvature. The maximum and minimum pressures (assuming unit density) for the normalized plot in Fig. 5 are 3.9 and 2.0 mbar, respectively. After 2.0 msec, the flow reverses and the drop returns to an oblate configuration.

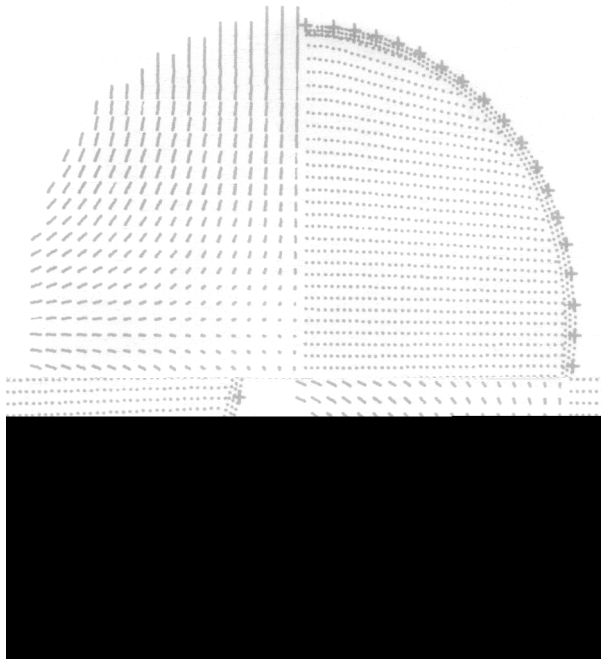

FIG. 6. Detail of Fig. 5 at $t = 1.0$ msec.

We note at $t = 0$ in Fig. 5 that the Rayleigh theory, which is not strictly valid for such large amplitudes, predicts a slight recurvature at the upper and lower poles. While it has been the experience here that the drop tends to return to very nearly its initial shape after one oscillation, this recurving feature does not reappear and is not physically realistic.

ACCURACY OF THE METHOD

It is appropriate to consider now various measures of the method's accuracy.

Conservation of Energy

While total momentum is rigorously conserved by the MAC difference equations (in the sense used in Ref. [28], and except in the vicinity of rigid walls, and except for the handling of free surfaces), quantities like volume and total energy are not. Conservation of these quantities depends on the overall accuracy of the computing scheme. The total energy is the sum of the kinetic energy K_e and the surface energy S_e (we exclude for the moment, the effect of viscosity which will tend to increase the internal energy at the expense of these other forms). Equation (18) has shown how S_e is related to the excess surface area of the drop. For the purpose of computing the drop area, we join adjacent pairs of surface particles with straight lines, each line segment thus forming the frustum of a cone in the cylindrical geometry of the present problem. Use is made of a simple expression which gives the lateral area of each frustum as a function only of the position of the pair of surface particles, and these areas can be easily found and summed to give the total. The reference area used for the calculation of S_e, ideally that of the equivalent sphere, is here taken to be the minimum area computed by this procedure during the oscillation.

The kinetic energy is given by

$$K_e = 1/2 \int \rho V^2 d(\text{volume}), \tag{22}$$

where V is the fluid speed, and the integral is taken over the whole drop. In evaluation of (22) it is natural to use the individual computing cell as the small increment of volume for the finite-difference summation. It should be noted, though, that if surface cells are treated for the purpose of this evaluation as being completely full of fluid, values of K_e will be computed which are too large. Tests have been conducted here which indicate that on the average for this geometry only about 25% of the surface cell volume should be used for computing K_e, and use of this fraction has given good results.

Figure 7 shows the variations of kinetic energy, surface energy, and their sum, the total energy, for the same calculations plotted in Fig. 5. The axial ratio of the drop γ is also shown as a function of time. As predicted by the Rayleigh theory, S_e and K_e behave like sine-squared functions. As the motion develops, the kinetic energy rises at the expense of surface energy and reaches a maximum at the spherical shape ($\gamma = 1.0$). The nonzero value of S_e after this first quarter cycle results from the use of the slightly smaller surface area, near $t = 3.1$ msec, in determining

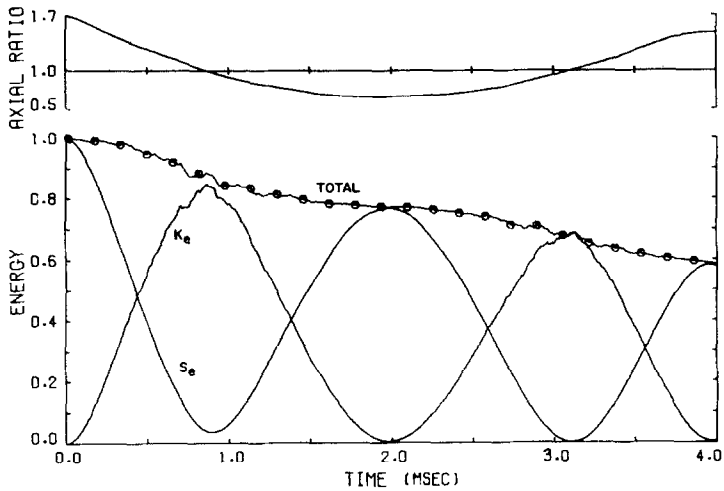

FIG. 7. Normalized kinetic, surface, and total energy, and axial ratio.

the surface energy reference level (level of zero potential energy). This change in the reference level can easily happen, since there is no guarantee that the drop will always pass through a spherical shape. In addition, such a change can result from very small changes in the drop volume. In this regard we note here that the excess surface energy S_e is only about 5% of the total surface energy σA_s for $\gamma = 1.7$ so that changes in drop volume of only a few tenths of a percent can account for the sort of variation in the zero surface energy level seen in Fig. 7.

As the drop enters the prolate configuration ($\gamma < 1$) the kinetic energy falls, going to very nearly zero, the surface energy reaches a maximum, and the drop comes to rest. Since K_e effectively reaches zero, it is clear that all volume elements come to rest at the same time, and hence, that this oscillation is indeed a normal mode. As shown also in Fig. 5, the flow then reverses and the same sequence of energy transformations is repeated for the second half of the cycle.

Viscous Dissipation

The viscous dissipation of kinetic energy causes gradual decreases in the total energy and amplitude of oscillation of the drop. In the calculation summarized in Fig. 7, 4.5×10^{-2} ergs, or about 40% of the initial total energy, is dissipated as heat during one oscillation. This amount of energy will raise the drop temperature by only a negligible amount, about 10^{-6}C, so that we can expect no interesting thermodynamic consequences from this generation of internal energy.

Comparison of the viscous dissipation observed in the numerical model with that given by Lamb's theory reveals only rough agreement. In all cases, the theory

predicts about 3–8 % more dissipation than takes place in the model. As examples, for a calculation with $d = 1.2$ mm, $\nu = 0.014$ cm^2 sec^{-1} and initial axial ratio $\gamma = 1.05$, the model gives b/b_0, the ratio of final to initial amplitude, as 0.96, whereas the theory predicts $b/b_0 = 0.93$. For $\gamma = 1.9$ and $\nu = 0.04$ cm^2 sec^{-1}, the model indicates $b/b_0 = 0.83$ and the theory gives 0.79. The worst agreement occurs for the case discussed above, with $\gamma = 1.7$ and $\nu = 0.06$ cm^2 sec^{-1}, the largest viscosity used, where model and theory give 0.80 and 0.72, respectively. While the theory is not expected to be accurate at large amplitudes, it should be quite adequate for $\gamma = 1.05$, and we conclude that the numerical model provides an insufficient amount of viscous dissipation. The zero-shear condition used by the MAC method in certain surface cells gives a constant bias in the proper sense to explain this problem, but does not appear to be quantitatively adequate.

Volume Conservation

The total drop volume has been determined by a Lagrangian technique involving summing the volumes of frustums of cones, much like the technique used for determining the surface area. The total volume, as measured by this technique, is conserved well by the computing scheme. During the calculation of a complete drop oscillation, amounting to about 500 computational time steps, the total volume is observed to change by no more than 0.8 %. Since the period of oscillation varies as the squareroot of the drop volume, negligible error in the computed period will result from this small change.

Asymmetric Character of Large-Amplitude Oscillation

It is interesting to note in Fig. 7 that the drop spends considerably more time in the prolate configuration that in the oblate (57 vs 43 %). This prediction of 14 % more time in the prolate shape is consistent with wind tunnel observations of oscillating drops made by Montgomery [19]. In the current work this excess time, expressed as a percentage, is observed to vary linearly with the amplitude of oscillation, expressed in terms of the maximum axial ratio, going to zero at $\gamma = 1.0$. Thus, at small amplitudes the model predicts symmetric oscillations in agreement with theory, and at large amplitudes it predicts asymmetric oscillations in agreement with observations.

Predicted Oscillation Period

As an additional measure of the accuracy of the numerical method, particularly with regard to the gross motion of the drop, we now consider the computed period of oblate–prolate oscillation. It is convenient to nondimensionalize the

problem so that the results are independent of the particular values assumed for the various parameters. Neglecting viscous effects, the important variables are: ρ, σ, R, and the period of oscillation τ. In addition to these we must include shape parameters d_1 and d_2, the major and minor axes of the drop. From these variables we can form the dimensionless quantities: $\tau(\rho R^3\sigma^{-1})^{-1/2}$ and d_1/d_2. The denominator of the first quantity is within a factor of $\pi/\sqrt{2}$ of the Rayleigh period τ_R, and we may equally well write the first group as τ/τ_R. The second group is simply the axial ratio γ. Dimensional analysis states that there must be a functional relation between the two quantities, and we choose to write it in the form $\tau/\tau_R = f(\gamma)$. Evaluation of this relationship should give all the information of interest.

Figure 8 shows $(\tau/\tau_R) - 1$, expressed as a percent, versus axial ratio, for

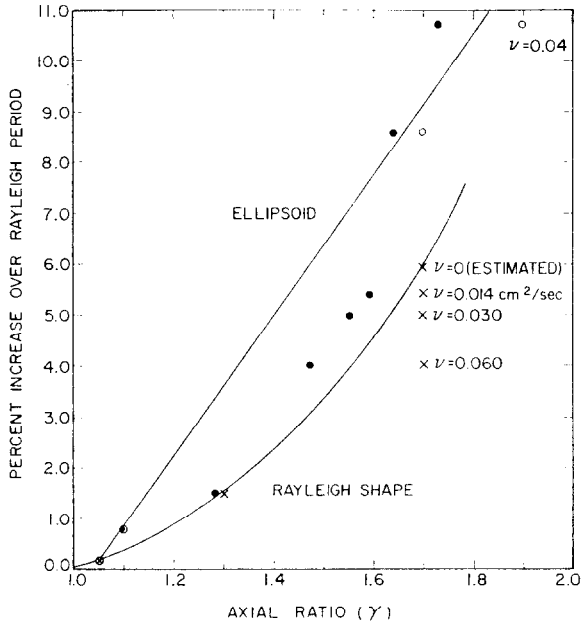

FIG. 8. Computed period of oscillation. The crosses and circles mark the start of a given calculation. The dots indicate the axial ratio at the end of one oscillation.

calculations made with both the Rayleigh shape and the elliptical shape. The curves approach the theoretical value for γ near 1.0, in agreement with the Rayleigh theory. For large axial ratio, the computed period is about 10% greater than the Rayleigh value. In a study of actual water drops, Montgomery [19] also observed roughly a 10% excess, so that the present computations are consistent with available experiment on this point. (It should be noted that most experiments,

e.g., Nelson and Gokhale [20], have not had sufficient accuracy to detect a deviation this small. Clearly, future experiments concerned with this problem will need to be capable of making measurements accurate to within at least a few percentage points).

Several features of Fig. 8 require comment. It is seen that the curve for the elliptical shape is above that for the Rayleigh shape. This results from the fact that a given γ, the two shapes do not have the same surface area. The elliptical shape has a larger area, undergoes a greater amount of distortion, and has a longer period of oscillation.

Although the computations are made with a finite viscosity (equal to 0.014 cm^2 sec^{-1}, except as otherwise indicated), an attempt is made to draw the curves in Fig. 8 for zero viscosity. As an example, three different viscosities are used at $\gamma = 1.7$ (Rayleigh shape), and the results are extrapolated to zero viscosity. Along with the initial axial ratio for each run, plotted as a circle or a cross, the axial ratio after the completion of one oscillation is plotted as a dot. As a result of the viscous dissipation, the final γ is always less than the initial. While viscosity tends to slow down fluid motion, we note here that computations using larger viscosities predict shorter periods. This is a result of the smaller average axial ratio in the large-ν case, and the positive slope of the curve in Fig. 8. Because of the viscosity-induced change in the amplitude of oscillation during a given calculation, we pass the curve through an average of the initial and final γ's.

An independent estimate of the Rayleigh period for an oscillation with amplitude corresponding to a maximum axial ratio of 1.7 has been made by Brazier-Smith (private communication) using a numerical potential flow model (for a description of this model see Brazier-Smith, Jennings and Latham [2]). Brazier-Smith's value and the estimate made here by extrapolating to zero viscosity agree to within 0.1 %.

On the basis of the results presented here, it is concluded that the numerical technique predicts quite realistically the motion of an oscillating drop, and one expects that it should be equally applicable to other types of problems involving drop distortions.

REFERENCES

1. D. C. BLANCHARD, The behavior of water drops at terminal velocity in air, *Trans. Amer. Geophys. Union* **31** (1950), 836.
2. P. R. BRAZIER-SMITH, S. G. JENNINGS AND J. LATHAM, An investigation of the behavior of drops and drop-pairs subjected to strong electrical forces, *Proc. Roy. Soc. London A*, **325** (1971), 363.
3. R. K.-C. CHAN AND R. L. STREET, A computer study of finite-amplitude water waves, *J. Comput. Phys.* **6** (1970), 68.
4. S. CHANDRASEKHAR, The oscillations of a viscous liquid globe, *Proc. London Math. Soc.* **9** (1959), 141.

5. B. J. DALY, A technique for including surface tension effects in hydrodynamic calculations, *J. Comput. Phys.* **4** (1969), 97.
6. B. J. DALY AND W. E. PRACHT, Numerical study of density-current surges, *Phys. Fluids* **11** (1968), 15.
7. B. A. FINLAY, A study of liquid drops in an air stream, Ph.D. dissertation, University of Birmingham, 1957.
8. G. B. FOOTE, A theoretical investigation of the dynamics of liquid drops, Ph.D. dissertation, University of Arizona, 1971.
9. F. H. GARNER AND J. J. LANE, Mass transfer to drops of liquid suspended in a gas stream, *Trans. Inst. Chem. Eng.* **37** (1959), 162.
10. F. H. HARLOW AND J. P. SHANNON, The splash of a liquid drop, *J. Appl. Phys.* **38** (1967), 3855.
11. F. H. HARLOW AND J. E. WELCH, Numerical calculation of time-dependent viscous incompressible flow of fluid with free surface, *Phys. Fluids* **8** (1965), 2182.
12. C. W. HIRT, Heuristic stability theory for finite-difference equations, *J. Comput. Phys.* **2** (1968), 339.
13. C. W. HIRT, J. L. COOK, AND T. D. BUTLER, A Lagrangian method for calculating the dynamics of an incompressible fluid with free surface, *J. Comput. Phys.* **5** (1970), 103.
14. H. LAMB, On the oscillations of a viscous spheroid, *Proc. London Math. Soc.* **13** (1881), 51.
15. H. LAMB, "Hydrodynamics," Dover Publications, New York, 1932.
16. L. D. LANDAU AND E. M. LIFSHITZ, "Fluid Mechanics," Addison–Wesley, Reading, MA, 1959.
17. D. K. LILLY, Numerical solutions for the shape-preserving two-dimensional thermal convection element, *J. Atmos. Sci.* **21** (1964), 83.
18. R. H. MAGARVEY AND B. W. TAYLOR, Free fall breakup of large drops, *J. Appl. Phys.* **27** (1956), 1129.
19. D. N. MONTGOMERY, private communication, 1969 also, D. N. MONTGOMERY, Collisional phenomena of uncharged water drops in a vertical electric field, Ph.D. dissertation, University of Arizona, 1968.
20. A. R. NELSON AND N. R. GOKHALE, Oscillation frequencies of freely suspended water drops, *J. Geophys. Res.* **77** (1972), 2724.
21. B. D. NICHOLS AND C. W. HIRT, Improved free surface boundary conditions for numerical incompressible-flow calculations, *J. Comput. Phys.* **8** (1971), 434.
22. D. W. PEACEMAN AND H. H. RACHFORD, The numerical solution of parabolic and elliptic differential equations, *J. Soc. Ind. Appl. Math.* **3** (1955), 28.
23. N. A. PHILLIPS, An example of non-linear computational instability, *in* "The Atmosphere and Sea in Motion," Rockefeller Institute Press in association with Oxford University Press, New York, 1959.
24. Lord Rayleigh, On the capillary phenomena of jets, *Proc. Roy. Soc. London* **29** (1879), 71.
25. W. H. REID, The oscillations of a viscous liquid drop, *Quart. Appl. Math.* **18** (1960), 86.
26. P. N. SWARZTRAUBER, A numerical model of the unsteady free boundary of an ideal fluid, *Quart. Appl. Math.* (in press).
27. J. L. WALSH, J. H. AHLBERG, AND E. N. NILSON, Best approximation properties of the spline fit, *J. Math. Mech.* **11** (1962), 225.
28. J. E. WELCH, F. H. HARLOW, J. P. SHANNON, AND B. J. DALY. "The MAC Method," Los Alamos Scientific Laboratory Report LA-3425, 1966.